

Supplemental Material for: Acoustic radiation force on a heated spherical particle in a fluid including scattering and microstreaming from a standing ultrasound wave

Bjørn G. Winckelmann* and Henrik Bruus†
*Department of Physics, Technical University of Denmark,
 DTU Physics Building 309, DK-2800 Kongens Lyngby, Denmark*
 (Dated: 29 June 2023)

This Supplemental Material provides MATLAB files for evaluating the acoustic contrast factor Φ_{ac} on a heated solid particle suspended in a fluid and located in a standing pressure wave. A COMSOL MULTIPHYSICS script that evaluates Φ_{ac} in this setting is also provided, and a description of the numerical simulation is given. We also show comparisons between the analytical results and the numerical simulations. Lastly, we comment on the temperature dependent material parameters used in our analysis.

S1. SUPPLEMENTAL FILES

In the Supplemental Material, we have included the files listed in Table S1. The MATLAB function `DOD1_0.m` calculates the force coefficients D_0^0 and D_1^0 and the function `DnDe1T0.m` calculates $D_n^{\Delta T}$. The MATLAB script `Phiac_PS_WA.m` computes the acoustic contrast factor Φ_{ac} for the case of a polystyrene particle suspended in water, which is the case shown in Fig. 2(a) of the main article, by using the two MATLAB functions `DOD1_0.m` and `DnDe1T0.m`. The file `Frad_gradT0.mph` is a COMSOL MULTIPHYSICS file used to compute the acoustic scattering, microstreaming, and Φ_{ac} on a heated polystyrene particle. In this script, the user can choose the fluid to be either water, ethanol, or oil.

TABLE S1. List of the MATLAB files and the COMSOL script provided in the Supplemental Material.

File name	File contents
<code>Phiac_PS_WA.m</code>	MATLAB script for computing Φ_{ac}
<code>DOD1_0.m</code>	MATLAB function for computing D_0^0, D_1^0
<code>DnDe1T0.m</code>	MATLAB function for computing $D_n^{\Delta T}$
<code>Frad_gradT0.mph</code>	COMSOL script for computing Φ_{ac}

S2. NUMERICAL SIMULATIONS IN COMSOL MULTIPHYSICS

In this section we briefly describe the COMSOL simulation implemented in the script file `Frad_gradT0.mph` and summarize the results of our numerical study. The different computational zones of the simulation and the referenced coordinate systems are shown in Fig. S1. We simulate the elastic solid at $0 < r < a$, the fluid at $a < r < R_{fluid}$, and a perfectly matched layer (PML)

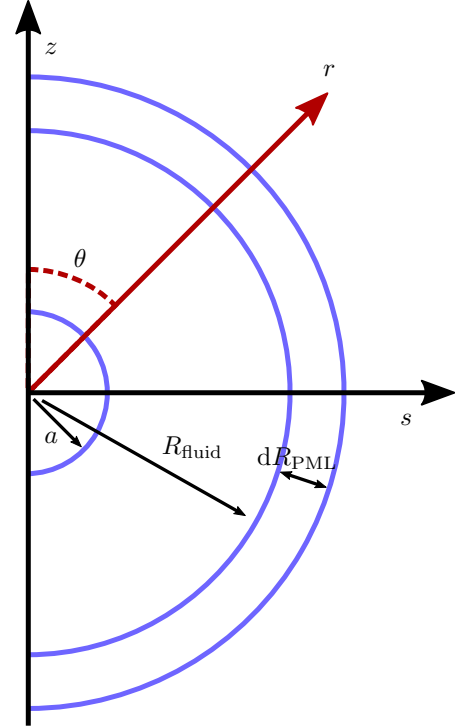


FIG. S1. Sketch of the simulated geometry and the referenced coordinate systems: cylindrical (s, z, φ) and spherical (r, θ, φ) .

at $R_{fluid} < r < R_{fluid} + dR_{PML}$. We use the symmetry of the problem around the central z -axis to keep the geometry two-dimensional.

The zeroth-order temperature field T_0 is governed by the equations,

$$\rho'_0 c'_{p0} \partial_t T'_0 = \nabla \cdot [k_0^{th} \nabla T'_0] + P_0, \quad 0 < r < a, \quad (S1a)$$

$$\rho_0 c_{p0} \partial_t T_0 = \nabla \cdot [k_0^{th} \nabla T_0], \quad a < r < R_{fluid}. \quad (S1b)$$

The particle and the surrounding fluid is assumed to initially be at ambient temperature T_0^∞ , and at time $t = 0$ the source of heating is activated. We apply continuity of

* winckel@dtu.dk

† bruus@fysik.dtu.dk

temperature and heat flux, and the temperature is held at T_0^∞ far from the sphere at $r = R_{\text{fluid}}$, leading to the following boundary conditions,

$$T_0(r, 0) = T_0'(r, 0) = T_0^\infty, \quad (\text{S2a})$$

$$T_0(a, t) = T_0'(a, t), \quad (\text{S2b})$$

$$k_0^{\text{th}} \partial_r T_0(a, t) = k_0^{\text{th}'} \partial_r T_0'(a, t), \quad (\text{S2c})$$

$$T_0(R_{\text{fluid}}, t) = T_0^\infty. \quad (\text{S2d})$$

The first-order fields \mathbf{u}_1 , \mathbf{v}_1^{sc} , and p_1^{sc} are computed from,

$$-\rho_0' \omega^2 \mathbf{u}_1 = \nabla \cdot \left\{ \rho_0' c_{\text{tr}0}^{\prime 2} \left[(\nabla \mathbf{u}_1) + (\nabla \mathbf{u}_1)^\top \right] + \rho_0' (c_{\text{lo}0}^{\prime 2} - 2c_{\text{tr}0}^{\prime 2}) (\nabla \cdot \mathbf{u}_1) \mathbf{I} \right\}, \quad 0 < r < a, \quad (\text{S3a})$$

$$\left(\frac{i\omega}{c_0^2} - \frac{i\omega}{c_{\infty 2}^2} \right) p_1^{\text{in}} + \frac{i\omega}{c_0^2} p_1^{\text{sc}} = (\rho_0 - \rho_0^\infty) \nabla \cdot \mathbf{v}_1^{\text{in}} + \rho_0 \nabla \cdot \mathbf{v}_1^{\text{sc}} + \nabla \rho_0 \cdot (\mathbf{v}_1^{\text{in}} + \mathbf{v}_1^{\text{sc}}), \quad a < r < R_{\text{fluid}} + dR_{\text{PML}}, \quad (\text{S3b})$$

$$-\text{i}\omega(\rho_0 - \rho_0^\infty) \mathbf{v}_1^{\text{in}} - \text{i}\omega \rho_0 \mathbf{v}_1^{\text{sc}} = \nabla \cdot \left\{ (\eta_0 - \eta_0^\infty) \left[(\nabla \mathbf{v}_1^{\text{in}}) + (\nabla \mathbf{v}_1^{\text{in}})^\top \right] + \left[(\eta_0^{\text{b}} - \frac{2}{3}\eta_0) - (\eta_0^{\text{b}\infty} - \frac{2}{3}\eta_0^\infty) \right] (\nabla \cdot \mathbf{v}_1^{\text{in}}) \mathbf{I} + \eta_0 \left[(\nabla \mathbf{v}_1^{\text{sc}}) + (\nabla \mathbf{v}_1^{\text{sc}})^\top \right] + (\eta_0^{\text{b}} - \frac{2}{3}\eta_0) (\nabla \cdot \mathbf{v}_1^{\text{sc}}) \mathbf{I} - p_1^{\text{sc}} \mathbf{I} \right\}, \quad a < r < R_{\text{fluid}} + dR_{\text{PML}}. \quad (\text{S3c})$$

We apply the boundary conditions of continuous velocity and stress at the particle boundary, and the scattered waves are damped in the PML layer far from the particle to avoid reflections,

$$-\text{i}\omega \mathbf{u}_1 = \mathbf{v}_1^{\text{sc}} + \mathbf{v}_1^{\text{in}}, \quad r = a, \quad (\text{S4a})$$

$$\boldsymbol{\sigma}'_1 \cdot \mathbf{n} = \boldsymbol{\sigma}_1 \cdot \mathbf{n}, \quad r = a, \quad (\text{S4b})$$

$$\partial_i \rightarrow \frac{1}{S(r)} \partial_i, \quad i = s, z, \quad r > R_{\text{fluid}}, \quad (\text{S4c})$$

$$di \rightarrow S(r) di, \quad i = s, z, \quad r > R_{\text{fluid}}, \quad (\text{S4d})$$

$$S(r) = 1 + \text{i}K_{\text{PML}} \left(\frac{r - R_{\text{fluid}}}{dR_{\text{PML}}} \right)^2. \quad (\text{S4e})$$

Here, K_{PML} defines the strength of the PML layer and is set to 4 in our simulations. The incident field is defined analytically as a standing plane wave,

$$p_1^{\text{in}} = p_a \cos [k_c(z + d)], \quad (\text{S5a})$$

$$\mathbf{v}_1^{\text{in}} = -\frac{i\omega}{\rho_0^\infty c_0^\infty k_c^2} \nabla p_1^{\text{in}}. \quad (\text{S5b})$$

Here, d defines the particle position in the pressure wave, which is chosen to be $d = \lambda_0/6 = c_0^\infty/(6f)$ in the simulations shown here.

The second-order fields $\langle \mathbf{v}_2 \rangle$ and $\langle p_2 \rangle$ are governed by

the following equations at $a < r < R_{\text{fluid}}$,

$$0 = \nabla \cdot \left\langle \rho_0 \mathbf{v}_2 + \frac{1}{c_0^2} (p_1^{\text{in}} + p_1^{\text{sc}}) (\mathbf{v}_1^{\text{in}} + \mathbf{v}_1^{\text{sc}}) \right\rangle, \quad (\text{S6a})$$

$$\mathbf{0} = \nabla \cdot \langle \boldsymbol{\sigma}_2 - \rho_0 (\mathbf{v}_1^{\text{in}} + \mathbf{v}_1^{\text{sc}}) (\mathbf{v}_1^{\text{in}} + \mathbf{v}_1^{\text{sc}}) \rangle, \quad (\text{S6b})$$

$$\langle \boldsymbol{\sigma}_2 \rangle = \eta_0 \left[\nabla \langle \mathbf{v}_2 \rangle + (\nabla \langle \mathbf{v}_2 \rangle)^\top \right] + (\eta_0^{\text{b}} - \frac{2}{3}\eta_0) (\nabla \cdot \langle \mathbf{v}_2 \rangle) \mathbf{I} - \langle p_2 \rangle \mathbf{I} + \left\langle \eta_1 \left[\nabla \mathbf{v}_1 + (\nabla \mathbf{v}_1)^\top \right] + (\eta_1^{\text{b}} - \frac{2}{3}\eta_1) (\nabla \cdot \mathbf{v}_1) \mathbf{I} \right\rangle. \quad (\text{S6c})$$

We apply the no-slip boundary condition at $r = a$ and a truncation of the time-averaged velocity field on the edge of the physical fluid domain,

$$\langle \mathbf{v}_2 \rangle|_{r=a} = -\langle (\mathbf{s}_1 \cdot \nabla) (\mathbf{v}_1^{\text{in}} + \mathbf{v}_1^{\text{sc}}) \rangle, \quad (\text{S7a})$$

$$\langle \mathbf{v}_2 \rangle|_{r=R_{\text{fluid}}} = \mathbf{0}. \quad (\text{S7b})$$

In defining the boundary condition for $\langle \mathbf{v}_2 \rangle$ on $r = R_{\text{fluid}}$, we have used the fact that a standing incident wave produces negligible streaming, so $\langle \mathbf{v}_2 \rangle$ is generated by the radially decaying scattered fields, which leads to a $\langle \mathbf{v}_2 \rangle$ that also decays away from the particle. The computational domain is then made sufficiently large so the outer boundary no longer affects the acoustic radiation force on the particle. All the equations and boundary conditions are implemented in the Weak Form PDE Interface of COMSOL MULTIPHYSICS.

In Figs. S2 and S3, we show results for simulations of a polystyrene sphere in water. The transient simulation of $T_0(\mathbf{r}, t)$ is stopped at $t = 1$ s, after which the acoustic problem is solved with the instantaneous profile of $T_0(\mathbf{r}, t)$ entering through the temperature dependencies of the material parameters. The power density in the solid is set to be adequate to reach an asymptotic surface temperature increase of $\Delta T_0^{\text{surf}} = 1$ K, the particle radius is set to $a = 2 \mu\text{m}$, the actuation frequency is $f = 1$ MHz, and the incident pressure amplitude is set to $p_a = 0.1$ MPa. We show comparisons between the simulated and analytically determined fields ΔT_0 , p_1^{sc} , and \mathbf{v}_1^{sc} along the two lines defined by $\theta = \frac{\pi}{4}$ and $\theta = \frac{\pi}{2}$. A good agreement between the simulated and the analytically known fields is observed, suggesting that our underlying assumptions are reasonable to zeroth and first

TABLE S2. Φ_{ac}^0 and $\Phi_{\text{ac}}^{\Delta T}(t = 1 \text{ s})$ obtained analytically from Eq. (51) and from the numerical simulations in COMSOL for a polystyrene particle of radius $a = 2 \mu\text{m}$ suspended in water, ethanol, and oil, respectively, and located in a standing incident wave with $f = 1$ MHz.

Parameter	Φ_{ac}^0	$\Phi_{\text{ac}}^{\Delta T}$	Fluid
COMSOL	0.173	0.215	Water
Analytical	0.172	0.233	Water
COMSOL	0.336	-0.331	Ethanol
Analytical	0.336	-0.311	Ethanol
COMSOL	-0.089	-0.300	Oil
Analytical	-0.090	-0.294	Oil

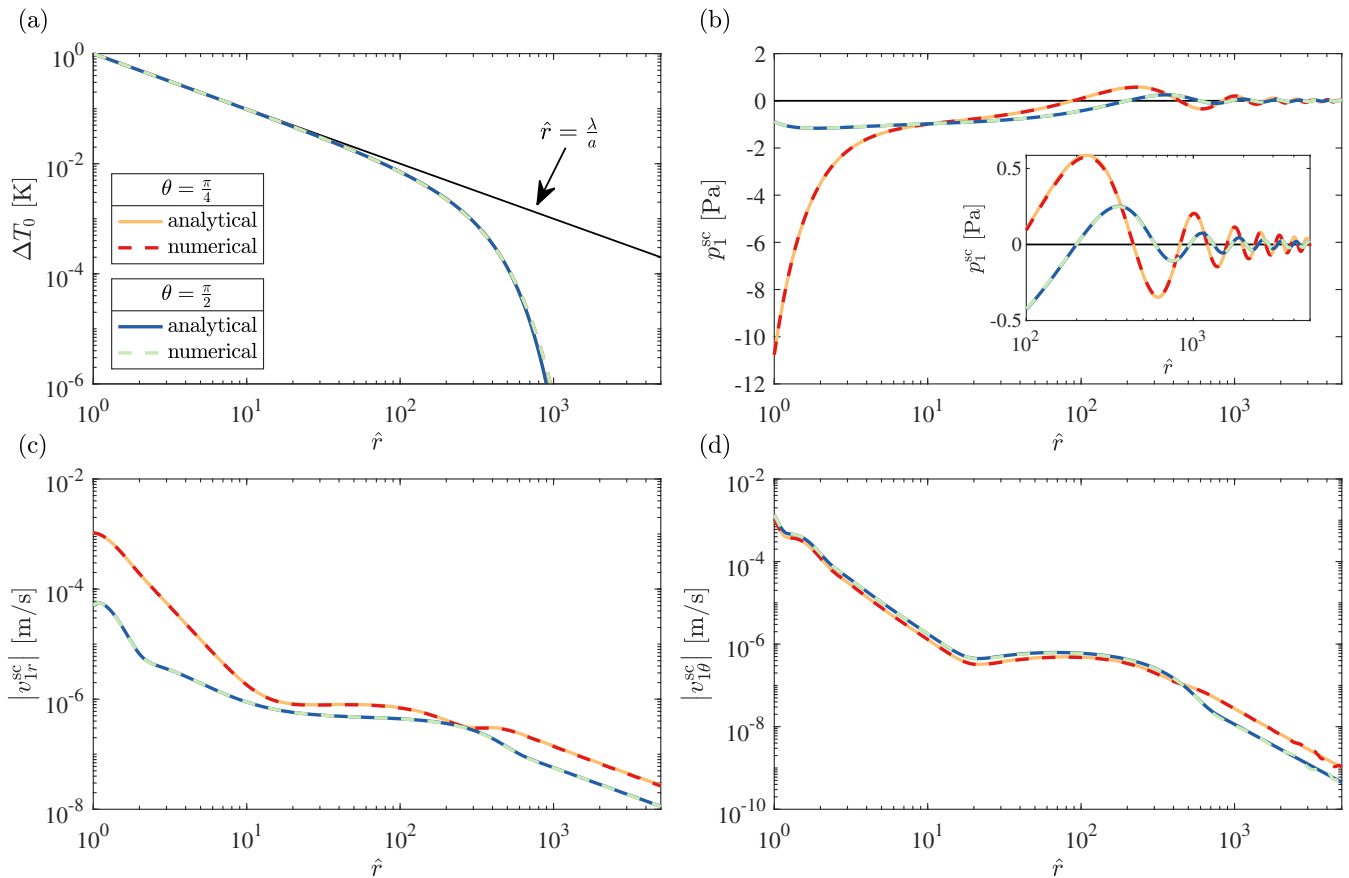


FIG. S2. Physical fields ΔT_0 , p_1^{sc} , and \mathbf{v}_1^{sc} plotted versus the normalized radial coordinate $\hat{r} = r/a$ calculated both from the analytical expressions of the main article and numerically in COMSOL. Plots are given along the two radial coordinates $\theta = \frac{\pi}{4}$ (orange full line analytical and red dashed line numerical) and $\theta = \frac{\pi}{2}$ (blue full line analytical and lightgreen dashed line numerical). The different plots compare: (a) ΔT_0 , (b) p_1^{sc} , (c) v_{1r}^{sc} , and (d) $v_{1\theta}^{\text{sc}}$. The inset in (b) show the far field of p_1^{sc} at $\hat{r} > 100$.

order. In the insets of Fig. S3, it is illustrated how the addition of $\Delta T_0 > 0$ adds long-reaching perturbations in the first-order fields. The same is true for the second-order velocity field $\langle \mathbf{v}_2 \rangle$, which we have illustrated with a surface plot in Fig. 3(b) in the main article. Here, we find that the streaming pattern transitions from a primarily quadrupole pattern to a more uni-directional pattern, when the particle is heated. The more asymmetric (around the particle equator) streaming pattern leads to a significant drag force contribution to \mathbf{F}^{rad} . In Table S2, we compare the numerical results obtained for Φ_{ac} in COMSOL to the analytical result from Eq. (51) found at $t = 1$ s for a polystyrene particle of radius $a = 2 \mu\text{m}$ suspended in water, ethanol, and oil, respectively. We find an almost perfect agreement for Φ_{ac}^0 , whereas the difference between COMSOL and analytical for $\Phi_{\text{ac}}^{\Delta T}$ is less than 10%, thus suggesting that the terms of primary importance are kept in our analysis. With this, we suggest that the primary perturbation to \mathbf{F}^{rad} obtained by heating the particle, will arise from long-range perturbations in our first-order fluid fields due to gradients in

the sound speed c_0 , that in turn perturb the streaming pattern $\langle \mathbf{v}_2 \rangle$ in the bulk of the fluid.

S3. TEMPERATURE DEPENDENT MATERIAL PARAMETERS

Here we comment on the temperature dependent parameters used in our COMSOL simulations. The material parameters of water are well known, and we use the polynomials from the appendix of Ref. [1].

For ethanol, we have taken expressions for η_0 , c_{p0} , and k_0^{th} as functions of T_0 directly from Ref. [2], and an expression for ρ_0 as a function of T_0 is taken directly from Ref. [3] Table 2. α_{p0} is found from this polynomial expression of ρ_0 by $\alpha_{p0} = -\frac{1}{\rho_0} \left(\frac{d\rho_0}{dT_0} \right)_p$. c_0 is found by making a second-order polynomial fit to the data taken from Ref. [4] Table 2 at atmospheric pressure (listed as 14.7 lb/in²). We could not find temperature dependent data for η_0^b , and a single temperature value is taken from Ref. [5]. The implications of this are expected to be

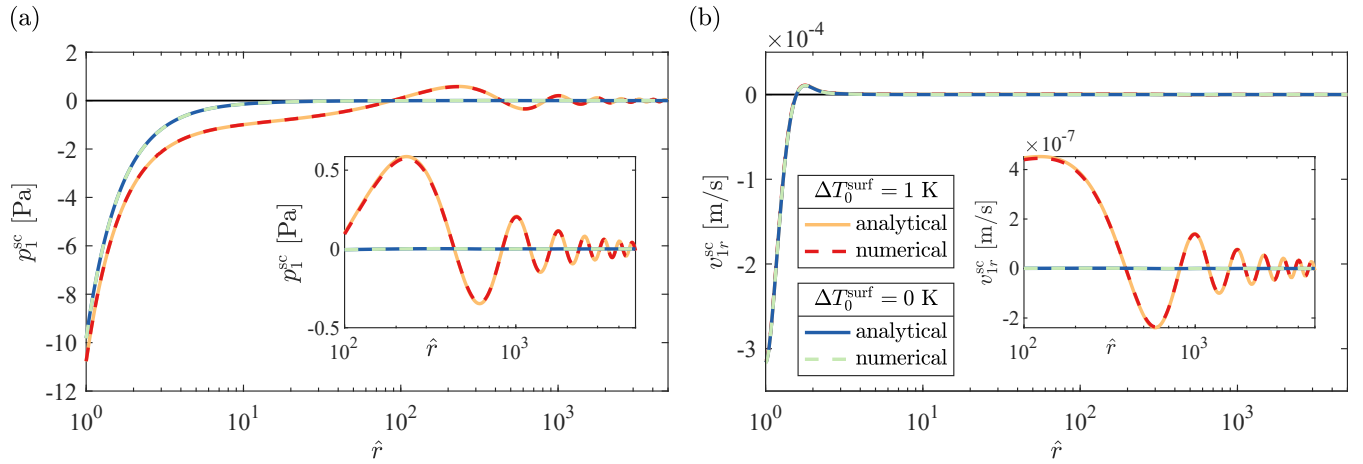


FIG. S3. Physical fields p_1^{sc} and v_{1r}^{sc} plotted versus the normalized radial coordinate $\hat{r} = r/a$ calculated both from the analytical expressions of the main article and numerically in COMSOL. Plots are given along the radial line defined by $\theta = \frac{\pi}{4}$ for $\Delta T_0^{\text{surf}} = 1 \text{ K}$ (orange full line analytical and red dashed line numerical) and $\Delta T_0^{\text{surf}} = 0$ (blue full line analytical and lightgreen dashed line numerical). The plotted fields are: (a) p_1^{sc} and (b) v_{1r}^{sc} . The insets show the far fields for $\hat{r} > 100$.

negligible.

For oil, we have compiled data to mimic a material reminiscent of an average food oil. Values for η_0 were taken from Table 1 in Ref. [6], where we excluded the outlier Lesquerella due its significantly higher viscosity. The viscosity data at each temperature point was then averaged for the remaining oils, and a fit was made to the expression $\eta_0 = A \exp(\frac{B}{C+(T_0-273.15[\text{K}])})$ suggested in Eq. (5) in Ref. [6]. Values for $\eta_0^b - \eta_0$ were taken from Table 4 and 5 of Ref. [7], and another fit of the type described above was found for this quantity. For ρ_0 , c_0 , and c_{p0} we used the expressions of Eqs. (1), (2), and (3) of Ref. [8] with the average values for the coefficients in the bottom of Table 2. k_0^{th} is reported to have negligible dependence on temperature, and the value for olive oil (which seemed reasonably average) in Table 1 of Ref. [8] was used. α_{p0} was again found from the relation $\alpha_{p0} = -\frac{1}{\rho_0} \left(\frac{d\rho_0}{dT_0} \right)_p$.

For oil and ethanol, we also used the identities,

$$\kappa_{s0} = \frac{1}{\rho_0 c_0^2}, \quad \gamma_0 = 1 + \frac{\alpha_{p0}^2 T_0}{\rho_0 c_{p0} \kappa_{s0}}. \quad (\text{S8})$$

For polystyrene, we have temperature dependent data for c_{p0} from Ref. [9] Table 3, to which we fit a fourth-order polynomial. We took temperature dependent data for c_{100} from Ref. [10] Table 1 (virgin sample) and fitted a linear polynomial to the data points for $T_0 < 90^\circ\text{C}$, after which the polystyrene is reported to undergo a glass transition. For the remaining parameters, we could not find temperature dependent data. However, for $c_{\text{tr}0}$ we assumed that the ratio $\frac{c_{100}}{c_{\text{tr}0}}$ is identical to the one reported in Ref. [11] at all temperatures. For ρ_0 we used the value given in Ref. [11] at $T_0^\infty = 300 \text{ K}$, and we then assumed the form $\rho_0 = \rho_0^\infty (1 - \alpha_{p0}^\infty \Delta T_0)$. For α_{p0} and k_0^{th} we assumed no temperature dependency and took single values from Ref. [12]. For polystyrene we also used the identities,

$$\kappa_{s0} = \frac{1}{\rho_0 (c_{100}^2 - \frac{4}{3} c_{\text{tr}0}^2)}, \quad \gamma_0 = 1 + \frac{\alpha_{p0}^2 T_0}{\rho_0 c_{p0} \kappa_{s0}}. \quad (\text{S9})$$

- [1] P. B. Muller and H. Bruus, Numerical study of thermoviscous effects in ultrasound-induced acoustic streaming in microchannels, *Phys. Rev. E* **90**, 043016 (2014).
- [2] *Pure Component Properties*, ChERIC, Chemical Engineering and Materials Research Information Center, <https://www.cheric.org/research/kdb/hcprop/showprop.php?cmpid=818>, accessed 13 May 2023.
- [3] T. Sun, J. Schouten, N. Trappeniers, and S. Biswas, Measurements of the densities of liquid benzene, cyclohexane, methanol, and ethanol as functions of temperature at 0.1

- mpa, *J. Chem. Thermodyn.* **20**, 1089 (1988).
- [4] W. Wilson and D. Bradley, Speed of sound in four primary alcohols as a function of temperature and pressure, *J. Acoust. Soc. Am.* **36**, 333 (1964).
- [5] A. S. Dukhin and P. J. Goetz, Bulk viscosity and compressibility measurement using acoustic spectroscopy, *J Chem Phys* **130**, 124519 (2009).
- [6] H. Nouredini, B. Teoh, and L. Davis Clements, Viscosities of vegetable oils and fatty acids, *J. Am. Oil Chem. Soc.* **69**, 1189 (1992).

- [7] S. Ghosh, M. Holmes, and M. Povey, Temperature dependence of bulk viscosity in edible oils using acoustic spectroscopy, *J. Food Process. Technol.* **8**, 1000676 (2017).
- [8] J. N. Coupland and D. J. McClements, Physical properties of liquid edible oils, *J. Am. Oil Chem. Soc.* **74**, 1559 (1997).
- [9] S. S. Chang and A. B. Bestul, Heat capacities for atactic polystyrene of narrow molecular weight distribution to 360 K., *J. Polym. Sci. A-2 Polym. Phys.* **6**, 849 (1968).
- [10] D. M. Smith and T. A. Wiggins, Sound speeds and laser induced damage in polystyrene, *Appl. Opt.* **11**, 2680 (1972).
- [11] *Tables of Acoustic Properties of Materials: Plastics*, Onda Corporation, <https://www.ondacorp.com/wp-content/uploads/2020/09/Plastics.pdf>, accessed 13 May 2023.
- [12] J. T. Karlsen and H. Bruus, Forces acting on a small particle in an acoustical field in a thermoviscous fluid, *Phys. Rev. E* **92**, 043010 (2015).